Nanorod Arrays

DOI: 10.1002/anie.201000783

Cerium Vanadate Nanorod Arrays from Ionic Chelator-Mediated Self-Assembly**

Junfeng Liu, Linlin Wang, Xiaoming Sun, and Xingqi Zhu*

Historically, there has been a constant effort to fabricate assembled regular superstructures from individual inorganic building blocks by "bottom-up" approaches.[1–7] Generally, monodisperse building blocks, modification of the colloid surface with long-tail surfactants, stable suspension in organic solvents, and controlled evaporation of solvent molecules have been considered as key factors for preparation of such superstructures.[3–5] In the last five years, alignment of non-spherical nanoparticles,[2] especially one-dimensional nanoparticles,[6,7] with intensified anisotropy has attracted vast attention, because such nanostructures allow investigation of the influence of size and dimensionality along with the collective optical and electronic properties of the particles, and they meet the needs of many practical applications.[8] However, the inert and insulating nature of surface organic ligands results in very poor interparticle coupling.[9] Construction of novel nanocrystal (NC) assemblies with active intermediate reagents remains a challenge. Very recently, a breakthrough was made by Kovalenko et al., who demonstrated that molecular metal chalcogenide complexes (MCCs) could stabilize colloids while preserving the ability of monodisperse NCs to form periodic structures (superlattices).[9] Herein, we report 1D $CeVO_4$ nanorod (NR) arrays in very salty aqueous solution from self-assembly under direction of an ionic multidentate ligand "glue", EDTA (ethylenediaminetetraacetic acid). Lanthanide orthovanadates are currently attracting broad attention owing to their prospective applications in many fields, for example as catalysts, laser host materials, and phosphors.[10–16] The ability to assemble lanthanide orthovanadate nanorod arrays should enable new types of applications with collective chemical and physical properties. Moreover, formation of such superstructures not only provides the opportunity to study the electronic communication between the NCs, but more importantly, it provides a new model for 1D nanostructure assembly and might lead to new directions for superstructure construction.

Assembly of $CeVO_4$ nanorods accompanied their hydrothermal synthesis from cerium nitrate and ammonium metavanadate with assistance from EDTA. After hydrothermal treatment at 180 °C for 6 h, brown aggregates formed at the bottom of the autoclaves. As-formed products had a sheet-like appearance in the low-magnification SEM image (Figure 1 a). A top view of the sheets demonstrates the striking long-range order of the assembly with a tetragonal close-packed arrangement of $CeVO_4$ NRs (Figure 1 b, only the square rod ends are visible). Figure 1 c gives the side view of the $CeVO_4$ NR arrays with several layers, thus indicating that the NRs ($l \approx 70$ nm, $d \approx 10$ nm) stand upright in the layer. The NRs are fairly uniform in each assembly and stack together in an ordered phase, forming a smectic-like structured superlattice, as schematically shown in the inset of Figure 1 d. Note that these assemblies often range over several micrometers (Figure 1 a), while only a small section of them is shown.

These side-by-side, assembled NRs are oriented approximately perpendicular to the layer, leading to a unusual X-ray diffraction (XRD) pattern of $CeVO_4$ superstructures (Figure 1 d) compared to the standard zircon-type pattern (space group $I4_1/amd$, JCPDS 79-1065). Peaks related to the *c* axis, including (112), (103), (204), and (004), were significantly strengthened, but (*h*,*k*,0) peaks, including (200) and (220), were obviously weakened. These results implied that the ⟨001⟩ crystal axis is perpendicular to the sheet plane of the NR array. In contrast, as the arrays were broken into individual rods and small bundles under repeated cycles of washing, sonication, and centrifugation (see the Supporting Information, Figure S1), the peak intensities become consistent with those in the JCPDS card. TEM and high-resolution TEM (HRTEM) gave further insight into the crystal structure and smectic-like assembly of $CeVO_4$ NRs (Figure 1 e–g). The multilayer arrays were exfoliated into single-layer sheets by dilution and weak sonication, which implied a weak interlayer interaction (see the Supporting Information, Figure S2). The low-magnification TEM image (Figure 1 e) and its fast Fourier transform (inset) demonstrated the long-range tetragonal packing order. The clear lattice fringes in the HRTEM images that were taken parallel and perpendicular to the *c* axis of individual NRs in the array (Figure 1 f,g) unambiguously demonstrated the exclusive growth of NRs along the *c* axis, as indicated by the arrow in Figure 1 g and in the model shown in the inset.

At the same time, HRTEM also revealed the existence of amorphous matter among the $CeVO_4$ NRs. Each rod in the array was separated by a regular spacing of about 3 nm (see

[*] Dr. J. F. Liu, L. L. Wang, Prof. X. M. Sun
State Key Laboratory of Chemical Resource Engineering
Beijing University of Chemical Technology
Beijing 100029 (China)
E-mail: sunxm@mail.buct.edu.cn
Dr. X. Q. Zhu
Anton-Paar China
Shanghai 200040 (China)

[**] This work was supported by the NSFC, the Beijing Natural Science Foundation, the Foundation for Authors of National Excellent Doctoral Dissertations of P. R. China, the Program for New Century Excellent Talents in Universities and the 973 Program (2009CB939802). The authors thank Prof. E. Q. Chen at Chemistry College of Peking University for SAXS testing.

Supporting information for this article is available on the WWW under http://dx.doi.org/10.1002/anie.201000783.

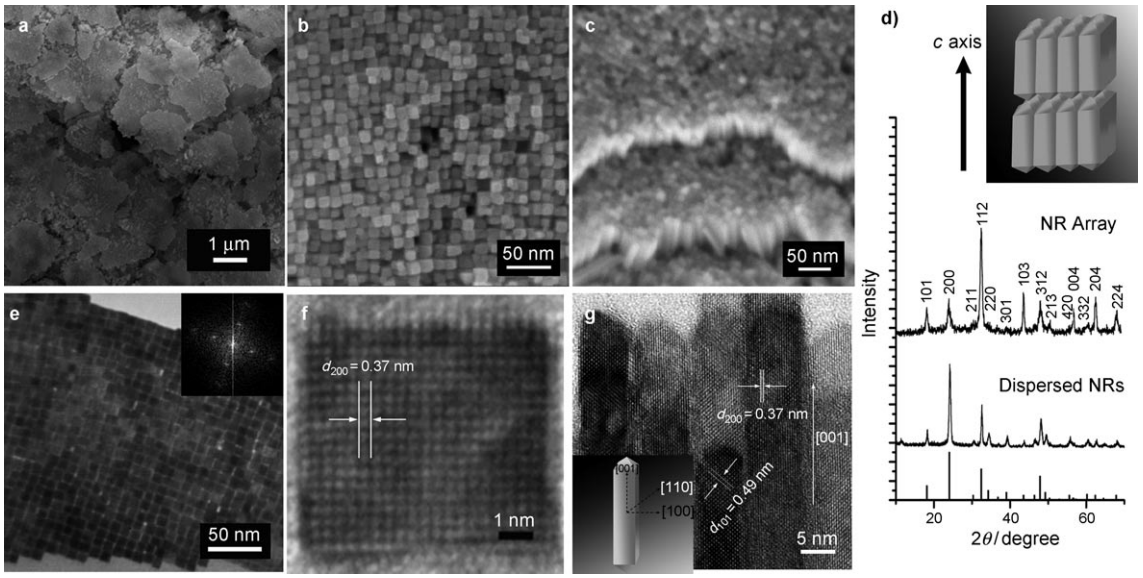

Figure 1. SEM images of a $CeVO_4$ NR array: a) Low-magnification image, b) top view, and c) side view. d) XRD patterns of a NR array (upper curve) and of individual NRs (middle curve), and standard lines from the JCPDS card (bottom lines). A schematic depiction of the array is shown in the inset. e) Low-magnification TEM image, with the fast Fourier transform in the inset. f) High-resolution image of individual NRs recorded along the *c* axis. g) High-resolution image of individual NRs recorded along the *a* or *b* axis.

the Supporting Information, Figure S3), a value which is about twice of the length of an EDTA molecule when it is completely extended. Raman spectra recorded on the NR array demonstrated the presence of EDTA molecules (Figure 2a). The peaks at 861, 799, 786, 461, and 370 cm^{-1} are assigned to the ν_1, ν_2, ν_3, and ν_4 modes of VO_4^{3-} ions.[17] The other peaks in the spectrum agree well with those of pure EDTA reported in the literature.[18] The C–C and C–N stretching vibrations result in intense Raman bands in the 900–1200 cm^{-1} spectral region (926, 966, 1052, and 1122 cm^{-1}); the C–H bands of the ethylene groups of EDTA are identified from the strong bands in the 2800–3100 cm^{-1} region. For comparison, we broke the NR assembly by repeated cycles of washing, sonication, and centrifugation.

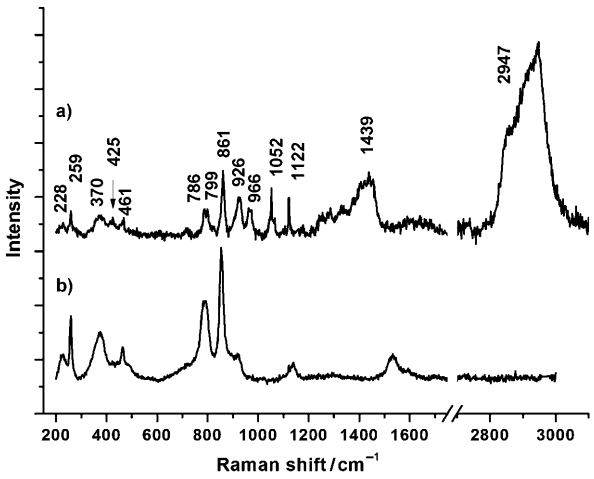

Figure 2. Raman spectrum of a) assembled $CeVO_4$ NR arrays and b) individual NRs after washing.

As-formed individual NRs and small bundles were also investigated using Raman spectroscopy (Figure 2b). It is seen clearly that only $CeVO_4$ vibrations are detected. The Raman spectra indicated that EDTA molecules are present in the NR arrays, and removal of them led to destruction of arrays, thus demonstrating the close relationship between EDTA and NR assembly.

To understand the growth process and the formation mechanism of assemblies, we carefully explored NR formation and assembly using TEM and SAXS (small-angle X-ray scattering) techniques (Figure 3). The initial reaction solution containing $Ce(NO_3)_3$, NH_4VO_3, and EDTA was clear because

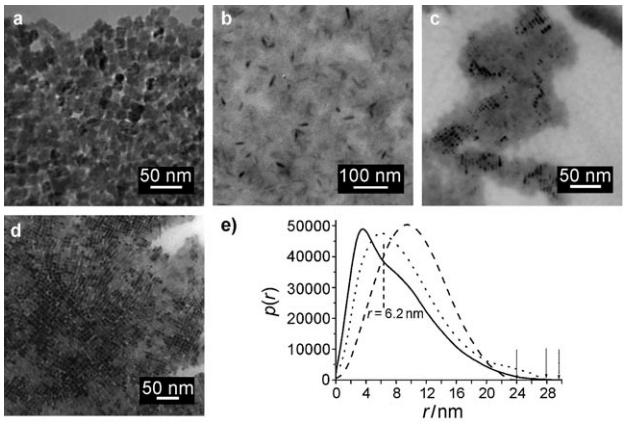

Figure 3. TEM images of $CeVO_4$ NR assemblies obtained at different reaction durations: a) 10, b) 15, c) 20, and d) 30 min. e) PDDFs ($p(r)$) of solutions at different reaction times: 10 (-----), 15 (••••), and 20 min (——). The arrows indicate the intercepts at the abscissa for the various samples. The $p(r)$ values for the 15 and 20 min experiments are multiplied by 2 and 5, respectively, in order to reach a similar height as the 10 min PDDF curve.

of the chelating effect of EDTA on Ce^{3+} ions. Under hydrothermal treatment, the Ce^{3+} EDTA complex had a greater chance of reacting with VO_4^{3-} to form initial colloidal $CeVO_4$ nuclei, as indicated by color change to brown after 5–10 min, since the chelation and capping capabilities of EDTA are effectively suppressed by raising the reaction temperature. But the nanoparticles formed at this stage are small, irregular, roughly spherical particles (Figure 3a). The amount of precipitation at this stage is so small that only harsh centrifugation for a long time produced visible aggregates. These initial colloidal precipitates, mediated by the adsorbed ligands on the crystal surface, can serve as the seeds for the growth of highly anisotropic nanostructures in the solution–solid process. As shown in Figure 3b, short 20 nm NRs ($d \approx 6.5$ nm) started to form in 15 min. After 20 min, the primary assembled arrays appeared (Figure 3c), but most of the arrays at this stage are monolayer ones with a scale of only several hundred nanometers, corresponding to a cluster of hundreds of NRs. Longer reaction times (e.g. 30 min) led to formation of NR assemblies with larger areas (Figure 3d); the diameters of the NRs simultaneously increase to about 9 nm. Larger $CeVO_4$ superstructures could be obtained by further extending the reaction time. These NR assemblies are so big and heavy that they spontaneously precipitated to the bottom of autoclaves.

SAXS confirmed the above growth procedure in the colloid solution state (Figure 3e). We performed SAXS experiments on the set of samples obtained at different reaction times and calculated the pair distance distribution functions (PDDFs) by fitting the scattering curves using the model-free GIFT method.[19] The point at which the PDDF curve decays down to zero reflects the maximum dimension of the particle (i.e., the length of individual rods). The almost symmetrical bell-shaped curve of the 10 min experiment is typical for sphere-like particles, which in this case have a maximum diameter of around 24 nm. Relative to the 10 min curve, the other PDDFs have their peaks shifted left, and the intercepts on the abscissa are shifted to larger values of r, that is, to larger maximum dimensions. The PDDF curve of the 15 min experiment is typical for prolate particles with a long axis of about 28 nm. The 20 min curve also shows a nearly triangle-shaped PDDF, which indicates 1D elongated (rod-like) particles. The inflection point in the decay part of the curve (marked by the vertical dashed line) indicates the diameter of the cross section, which is about 6.2 nm, consistent with our TEM results. The intercept (see arrow) represents the rod length ($r \approx 30$ nm). Normally, the decay in the PDDF of a cylinder is a straight line, which cannot be observed in our 15 and 20 min experiments. Reasons for these deviations are polydispersity in length and cross-section diameter as well as a small fraction of neighboring particles that are loosely attached to each other. In short, after a reaction time of 10 to 20 min, the particles transform from spheres through prolate particles and finally to rods with increasing axial ratios. In this process, the long axis of these particles increases gradually from 24 to 30 nm and can even exceed the resolution limit of the SAXS apparatus.

Accompanying the shape evolution, pH value change during the reaction was also observed. The pH value of the reaction mixture was adjusted to 10 at the beginning of the reaction. It dropped to 9.6 at 20 min and gradually to 8.6 at 6 h. In this range, vanadate exists mainly as protonated HVO_4^{2-}.[20] In consequent hydrothermal reaction, it transforms to $CeVO_4$ and releases H^+, as shown in Equations (1)–(4):

$$[CeEDTA]^- \rightleftharpoons Ce^{3+} + EDTA^{4-} \quad (1)$$

$$HVO_4^{2-} \rightleftharpoons H^+ + VO_4^{3-} \quad (2)$$

$$Ce^{3+} + VO_4^{3-} \rightleftharpoons CeVO_4 \downarrow \quad (3)$$

$$H^+ + EDTA^{4-} \rightleftharpoons HEDTA^{3-} \quad (4)$$

As the precipitation reaction in Equation (3) proceeds, it promotes the reactions in Equations (1) and (2). Released $EDTA^{4-}$ and H^+ combine to form $HEDTA^{3-}$ ions [Eq. (4)], which lead to a decrease of the pH value to near neutral. On the basis of the above considerations, we gain a preliminary understanding of the growth and self-assembly of $CeVO_4$ NRs (Figure 4). During the reaction process, VO_3^- is first transformed to HVO_4^{2-} in solution as the pH value is adjusted to 10.[20] EDTA is in stoichiometric excess to Ce^{3+} in the system, which enables Ce^{3+} to form complexes ($[CeEDTA]^-$) and be stabilized at room temperature. Under hydrothermal treatment, the $[CeEDTA]^-$ complex reacts with HVO_4^{2-} to form initial colloidal $CeVO_4$ nuclei [Eqs. (1)–(3), stage A in Figure 4] and releases free H^+ and $EDTA^{4-}$ [Eqs. (1) and (2)]. $EDTA^{4-}$ dissociates from the Ce^{3+} ions and preferentially binds to the (100) an (010) crystal faces of the cerium orthovanadate nuclei, thus resulting in the anisotropic growth of nanostructures along the c axis (stage B in Figure 4). By this means of growth, the final square rods are obtained, and the generated short NRs are covered by $EDTA^{4-}$ ions. More H^+ ions are released [Eq. (2)], leading to a decrease in the pH value and protonation of $EDTA^{4-}$. $HEDTA^{3-}$ eventually becomes the main form as the pH value decreases to 8.6. Hydrogen bonds form between two $HEDTA^{3-}$ ions on the surface of different $CeVO_4$ NRs, leading to self-assembly of

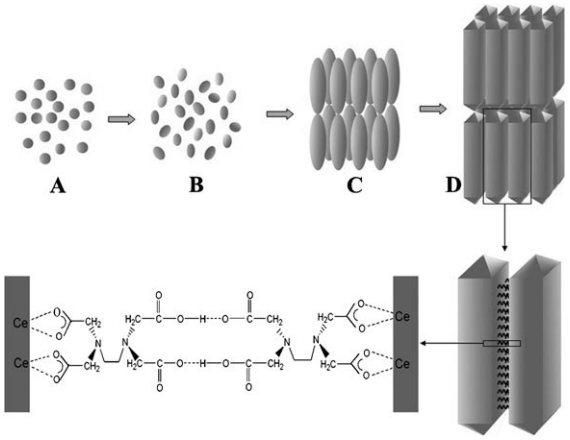

Figure 4. Growth and assembly of $CeVO_4$ NRs.

primary NRs (stage C in Figure 4). The primarily assembled NRs continuously grow, forming the final array of NRs after 6 h (stage D in Figure 4).

EDTA has been used in previous investigations to control the synthesis of rare-earth vanadate NRs[21–23] by decreasing the nanocrystal nucleation rate and by preferentially capping specific nanocrystal surfaces.[22] But there were no reports on assembly of such anisotropic building blocks. This lack is possibly due to the necessary strictly confined synthetic conditions, as our repeated experiments revealed. For instance, when $[Ce^{3+}] = 80$ mM, the most repeatable molar ratio was Ce:V:EDTA = 1:1:1.25. Even 10% deviation led to free individual nanorods or to formation of nanosheaves. Detailed results will be reported elsewhere.

In summary, we have demonstrated a facile and effective solution-phase approach to the synthesis of $CeVO_4$ NR arrays. The NRs were fairly uniform in size, growing along the [001] direction, and stacked together side-by-side in an ordered phase, forming a smectic-like structured array with several layers. The growth and assembly mechanism have been investigated in detail with TEM, HRTEM, SAXS, and Raman spectroscopy, which showed the important roles of EDTA molecules in the whole process: 1) chelating the Ce^{3+} ions in solution to decrease the nanocrystal nucleation rate; 2) controlling the anisotropic growth by restricting the active points of certain faces; 3) mediating the assembly by forming intermolecular hydrogen bonds. Our results might offer more opportunities to nanoscience and nanotechnology for bottom-up approach based on uniform NC building blocks.

Experimental Section

All reagents were purchased from Beijing Chemicals Co. Ltd. and used as received without further purification. In a typical synthesis, $Ce(NO_3)_3{\cdot}6H_2O$ (3.2 mmol) and EDTA (4.0 mmol) were dissolved in H_2O (10 mL), forming a chelated cerium complex. After vigorous stirring of the solution for several minutes, NH_4VO_3 (3.2 mmol) dissolved in H_2O (10 mL) was added. Subsequently, the pH value of the solution was adjusted to 10 with an appropriate amount of aqueous NaOH. Afterward, the mixture was transferred into a 40 mL Teflon-lined stainless steel autoclave, sealed tightly, and maintained at 180 °C for 6 h. The autoclave was left to cool to room temperature, and the precipitated powders were separated by centrifugation, washed with anhydrous ethanol several times, and dried at 70 °C for 12 h. Products were characterized by XRD, SEM, TEM, HRTEM, and SAXS. Detailed characterization methods can be found in the Supporting Information.

Received: February 9, 2010
Published online: April 6, 2010

Keywords: arrays · cerium · nanostructures · self-assembly · vanadates

[1] O. D. Velev, A. M. Lenhoff, E. W. Kaler, *Science* **2000**, *287*, 2240.
[2] T. Ding, K. Song, K. Clays, C.-H. Tung, *Adv. Mater.* **2009**, *21*, 1936.
[3] F. Bai, D. Wang, Z. Huo, W. Chen, L. Liu, X. Liang, C. Chen, X. Wang, Q. Peng, Y. Li, *Angew. Chem.* **2007**, *119*, 6770; *Angew. Chem. Int. Ed.* **2007**, *46*, 6650.
[4] J. Zhuang, A. D. Shalle, J. Lynch, H. Wu, O. Chen, A. D. Q. Li, Y. C. Cao, *J. Am. Chem. Soc.* **2009**, *131*, 6084.
[5] Y. Zhao, K. Thorkelsson, A. J. Mastroianni, T. Schilling, J. M. Luther, B. J. Rancatore, K. Matsunaga, H. Jinnai, Y. Wu, D. Poulsen, J. M. J. Fréchet , A. P. Alivisatos, T. Xu, *Nat. Mater.* **2009**, *8*, 979.
[6] N. Zhao, K. Liu, J. Greener, Z. Nie, E. Kumacheva, *Nano Lett.* **2009**, *9*, 3077.
[7] G.-M. Andrés, P.-J. Jorge, C. A. Enrique, T. Gloria, L.-M. Luis, *Angew. Chem.* **2009**, *121*, 9648; *Angew. Chem. Int. Ed.* **2009**, *48*, 9484.
[8] A. I. Hochbaum, P. Yang, *Chem. Rev.* **2010**, *110*, 527.
[9] M. V. Kovalenko, M. Scheele, D. V. Talapin, *Science* **2009**, *324*, 1417.
[10] J. Liu, W. Chen, X. Liu, K. Zhou, Y. Li, *Nano Res.* **2008**, *1*, 46.
[11] Z. M. Fang, Q. Hong, Z. H. Zhou, S. J. Dai, W. Z. Weng, H. L. Wan, *Catal. Lett.* **1999**, *61*, 39.
[12] M. V. Martinez-Huerta, J. M. Coronado, M. Fernandez-Garcia, A. Iglesias-Juez, G. Deo, J. L. G. Fierro, M. A. Banares, *J. Catal.* **2004**, *225*, 240.
[13] R. A. Fields, M. Birnbaum, C. L. Fincher, *Appl. Phys. Lett.* **1987**, *51*, 1885.
[14] A. Huignard, T. Gacoin, J. P. Boilot, *Chem. Mater.* **2000**, *12*, 1090.
[15] J. F. Liu, Y. D. Li, *Adv. Mater.* **2007**, *19*, 1118.
[16] J. F. Liu, Y. D. Li, *J. Mater. Chem.* **2007**, *17*, 1797.
[17] U. Opara Krasovec, B. Orel, A. Surca, N. Bukovec, R. Reisfeld, *Solid State Ionics* **1999**, *118*, 195.
[18] E. Faulques, D. L. Perry, S. Lott, J. D. Zubkowski, E. J. Valente, *Spectrochim. Acta Part A* **1998**, *54*, 869.
[19] O. Glatter, O. Kratky, *Small Angle X-ray Scattering*, Academic Press, London, **1982**.
[20] A. G. Sykes, *Adv. Inorg. Chem.* **1999**, *49*, 127.
[21] C. J. Jia, L. D. Sun, L. P. You, X. C. Jiang, F. Luo, Y. C. Pang, C. H. Yan, *J. Phys. Chem. B* **2005**, *109*, 3284.
[22] H. Deng, C. Liu, S. Yang, S. Xiao, Z.-K. Zhou, Q.-Q. Wang, *Cryst. Growth Des.* **2008**, *8*, 4432.
[23] F. Luo, C. J. Jia, W. Song, L. P. You, C. H. Yan, *Cryst. Growth Des.* **2005**, *5*, 137.

